J Mol Model (2011) 17:3241–3250
DOI 10.1007/s00894-011-1011-x

ORIGINAL PAPER

A combined molecular modeling study on a series of pyrazole/isoxazole based human Hsp90α inhibitors

Ying Yang · Huanxiang Liu · Juan Du · Jin Qin · Xiaojun Yao

Received: 25 November 2010 / Accepted: 6 February 2011 / Published online: 4 March 2011

Abstract Inhibition of the protein chaperone Hsp90α is a promising approach for cancer therapy. In this work, a molecular modeling study combining pharmacophore model, molecular docking and three-dimensional quantitative structure-activity relationships (3D-QSAR) was performed to investigate a series of pyrazole/isoxazole scaffold inhibitors of human Hsp90α. The pharmacophore model can provide the essential features required for the biological activities of the inhibitors. The molecular docking study can give insight into the binding mode between Hsp90α and its inhibitors. 3D-QSAR based on CoMFA and CoMSIA models were performed from three different strategies for conformational selection and alignment. The receptor-based models gave the most statistically significant results with cross-validated q^2 values of 0.782 and 0.829 and r^2 values of 0.909 and 0.968, for CoMFA and CoMSIA respectively. Furthermore, the 3D contour maps superimposed within the binding site of Hsp90α could help to understand the pivotal interaction and the structural requirements for potent Hsp90α inhibitors. The results show 4-position of pyrazole/isoxazole ring requires bulky and hydrophobic groups, and bulky and electron repulsion substituent of 5-amides is favorable for enhancing activity. This study will be helpful for the rational design of new potent Hsp90α inhibitors.

Keywords Alignment · CoMFA · CoMSIA · Hsp90α inhibitors · Molecular docking · Pharmacophore model

Electronic supplementary material The online version of this article (doi:10.1007/s00894-011-1011-x) contains supplementary material, which is available to authorized users.

Y. Yang · J. Du · J. Qin · X. Yao
State Key Laboratory of Applied Organic Chemistry and Department of Chemistry, Lanzhou University, Lanzhou 730000, China

H. Liu
School of Pharmacy, Lanzhou University, Lanzhou 730000, China

X. Yao (✉)
Key Lab of Preclinical Study for New Drugs of Gansu Province, Lanzhou University, Lanzhou 730000, China
e-mail: xjyao@lzu.edu.cn

Introduction

Heat shock protein 90 (Hsp90) belongs to the family of molecular chaperones, regulating the conformational maturation, stability and function of many important "client" proteins such as kinases, steroid hormone receptors, and transcription factors involved in cancer [1, 2]. The inhibition of Hsp90 can deliver a powerful anti-cancer effect through the combinatorial depletion of multiple oncogenic client proteins and the consequent modulation of all the hallmark traits of cancer cells. There exists two isoforms of Hsp90, i.e., α and β isoforms. Due to the discovery and characterization of two natural product inhibitors *geldanamycin* and *radicicol* [3], Hsp90α has emerged as an exciting target for the development of cancer chemotherapeutics [4]. Subsequently, based on the structural features of the N-terminal binding of ATP to Hsp90α, several small-molecule inhibitors were designed and synthesized, mainly including the purine and pyrazole/isoxazole scaffold [5–8].

Nowadays, molecular modeling techniques have been emerged as an important tool for drug design as they can provide quantitative structure-activity relationships of bioactive inhibitors and the information about target-drug interaction [9–15]. Many successful applications in medicinal chemistry can demonstrate the importance of these

methods in drug discovery and development [16–19]. As Hsp90α is an attractive target, the urgent need for novel anticancer agents has impelled to understand the structural requisites of promising inhibitors at the molecular level. Therefore, molecular modeling study and in silico design of small molecules inhibiting Hsp90 has aroused great interests [20–22].

However, understanding the impact of molecular flexibility of inhibitors remains an important problem in computer-aided drug design, as it can help assess the influence of bioactive conformation and pharmacophore features on the inhibition process. In order to consider the influence of the flexibility of the inhibitors during its interaction with the targets, molecular modeling techniques such as pharmacophore modeling, flexible docking and molecular dynamics simulation have been applied in the development of drug design [15, 20, 22]. In this study, we aimed to perform a combined molecular modeling study using pharmacophore modeling, molecular docking and 3D-QSAR on a series of pyrazole/isoxazole scaffold Hsp90α inhibitors from both ligand-based and structure-based methods. Considering the structural flexibility and diversity of the studied inhibitors, we proposed different strategies for conformational selection and alignment from pharmacophore and docking to develop 3D-QSAR models. The results could provide the information about the interaction between inhibitors and human Hsp90α, and gain insights to the structural requirements for inhibitory activity.

Materials and methods

Data set and molecule preparation

In this study, a series of 94 molecules as Hsp90α inhibitors were taken from the literatures [23–26]. The in vitro inhibitory activities (IC_{50}, in units of μM) were transformed to negative logarithmic units marked as pIC_{50} used as dependent variables in the CoMFA and CoMSIA analyses and pharmacophore modeling. The 3D structures were sketched in SYBYL 6.9 [27]. Partial atomic charges were calculated using Gasteiger–Hückel method, and energy minimization was performed using the Tripos force field with convergence criterion of 0.01 kcal mol^{-1}. Selection of the training set and the test set was done by considering the similar structural diversity and range of bioactivities of both sets. The data set was divided into a training set of 74 molecules and a test set of the remaining 20 molecules (Table S1 in Supporting information).

Generation of pharmacophore model

The pharmacophore model for Hsp90α inhibitors was generated using Phase [28]. A pIC_{50} value of 7.0 was chosen as the threshold for defining an active molecule by considering the activity range. Conformations for the studied molecules were generated by torsional search method with distance-dependent dielectric solvation treatment and OPLS-2001 force field. Five pharmacophore features were defined, namely hydrogen bond acceptor (A), hydrogen bond donor (D), hydrophobic group (H), positively charged group (P), and aromatic ring (R). Then common pharmacophore hypotheses (CPH) was examined using a survival scoring function to yield the best alignment of the active molecules. The resulting pharmacophore with high-ranking scores were validated by a partial least squares (PLS) regression-based cross-validation [29].

Molecular docking

We carried out the molecular docking simulation using Glide program [30]. The crystal structure of human Hsp90α N-terminal domain in complexes with ligand (corresponding to molecule **2**), was obtained from the Protein Data Bank (PDB code: 2BSM). The protein structure was prepared in Maestro [31]. Water molecules were removed from the complex except for three structurally conserved and highly ordered water molecules involved in the network with Asp93 at the ATP binding site, which are determined in all nine X-ray crystal structures of Hsp90α complexed with this pyrazole/isoxazole scaffold inhibitors (PDB codes: 2BT0, 2BSM, 2BYH, 2BYI, 2CCS, 2CCU, 2CCT, 2VCI and 2VCJ). Both protein and ligand were assigned partial charges using the OPLS-2005 force field. Then energy minimization was carried out to relax the structure [32]. The co-crystal ligand was used to determine the location of a docking grid box and was then removed prior to grid generation in the next step. After docking calculation, at most ten poses per ligand were generated. The best docked pose was chosen using Glide XP (extra precision) score [33, 34].

3D-QSAR models derived from three different strategies

Our CoMFA and CoMSIA analyses were performed using SYBYL 6.9. As the molecular conformation and alignment of molecules are two sensitive input parameters affecting the 3D-QSAR models, we used the following three different strategies to obtain bioactive conformations and generate alignments in this work.

Lowest-energy conformation and common scaffold based alignment (CBA)

The lowest-energy conformers represent the global minimum of the ligand, and may be the bioactive conformations [35]. To get a reasonable energy-lowest conformation for

each molecule, the conformational search was carried out using the multisearch routine in SYBYL 6.9. The most active molecule **62** was used as a template to align the remaining molecules by atom-by-atom fits (Fig. 1).

Pharmacophore-based conformational generation and alignment (PBA)

Pharmacophore model constitutes a useful tool to guide the alignment of flexible and diverse molecules in CoMFA and CoMSIA studies [36–39]. In our study, structurally different molecules were superimposed on the best pharmacophore model according to the same 3D chemical features rather than atom-by-atom comparison. The conformation of each molecule was selected based on the fitness score between the pharmacophoric features and the corresponding functional groups presented in the molecule.

Docking-based conformational generation and alignment (DBA)

The docking-based QSAR study has the advantages by taking features of the binding pocket of receptor to get the active conformation [40–44]. This method represents ligand-receptor interactions avoiding the bias that can be introduced by relying on ligand-based alignment. Here we derived this information directly from our Glide XP docking study.

The final aligned conformations of all molecules from three strategies were exported for 3D-QSAR modeling. The aligned training set molecules were placed in a 3D grid box ensuring the entire set included. The CoMFA [45] steric and electrostatic field energies between the probe and molecule at each lattice intersection were calculated with a grid step size of 2 Å using sp^3 C^+ as probe atom, which were automatically generated by the CoMFA-STD method with default energy of 30 kcal mol^{-1}. And in the case of CoMSIA models, steric, electrostatic, hydrophobic, hydrogen bond donor and hydrogen bond acceptor fields, were derived according to the method developed by Klebe et al. [46] with the same lattice box and probe atom used in the CoMFA calculations.

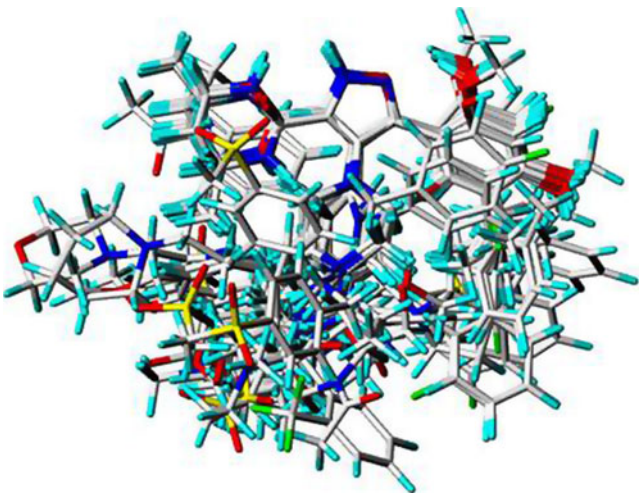

Fig. 1 Alignment of all 94 molecules using the lowest-energy conformers by atom fit

Then the performance of models was calculated by the leave-one-out (LOO) cross-validation using partial least squares (PLS) method [29, 47, 48]. The optimal number of components (ONC) obtained, which is equal to the number yielding the highest cross-validated coefficient q^2, was used to generate the final regression models by a non-cross-validated PLS analysis. And the conventional correlation coefficient r^2 and its standard error of estimation (SEE) were subsequently computed for the final PLS models. In addition, the boot strapping analysis [48] was carried out 100 times to validate each model. CoMFA and CoMSIA coefficient maps were generated by interpolation of the pairwise products between the PLS coefficients and the standard deviations of the corresponding CoMFA or CoMSIA descriptor values. The activities of the test set molecules were predicted to evaluate the predictive power of the built models with the correlation coefficient r^2_{pred}.

Results and discussion

Pharmacophore modeling

We obtained an AADRR pharmacophore model, including two hydrogen bond acceptors (A), one hydrogen bond donor (D) and two aromatic rings (R) features. Fig. 2a shows the pharmacophore hypotheses with the active molecules in the training and test sets aligned. It seemed that the alignment was very good when the high bioactive conformations were automatically aligned to the pharmacophore model, especially for the reference molecule **9** exactly matching with a fitness of three. For those molecules with poor inhibitory activity, they can only produce relatively good fits with three or two features. However, for the conformations not matching well, it should be manually adjusted for the alignment of further CoMFA and CoMSIA studies [36]. From the chemical intuition, the two common core structures, 3-resorcinol and pyrazole/isoxazole ring of these molecules should adopt similar orientation. Thus, in the adjustment, the R and A features corresponding to the pyrazole/isoxazole ring and the *para*-position O of 3-resorcinol were adopted as the criteria for all molecules superimposed in the similar space orientations. Then QSAR models were built based on this pharmacophore model.

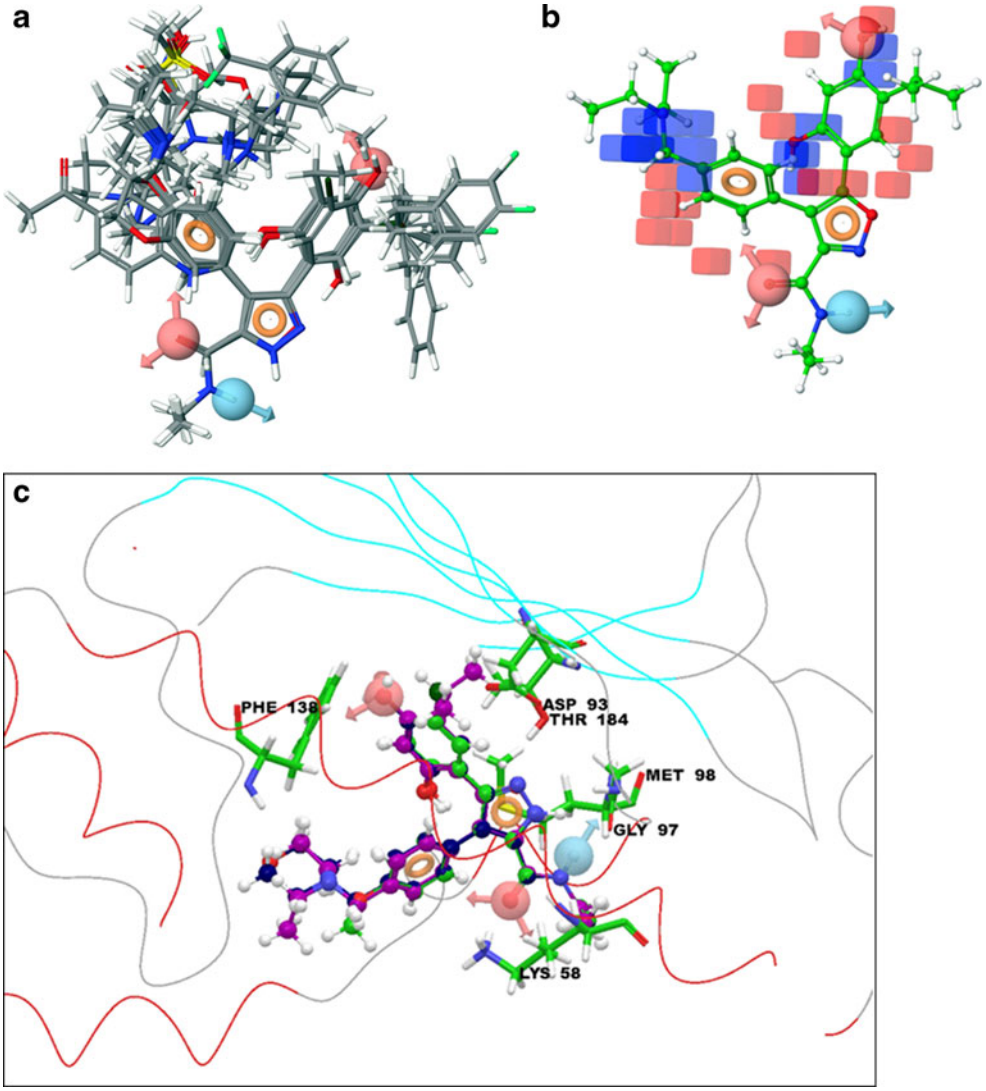

Fig. 2 (**a**) The alignment of active molecules by Phase pharmacophore hypothesis. H-bond acceptor (A): light red sphere with arrows; H-bond donor (D): light blue sphere with arrow; Atomatc ring (R): orange torus in the plane of the ring. (**b**) Visual representation of atom-based Phase QSAR with all atom classes, aligned with molecule **62**. Blue cubes are favorable regions for activity, and red cubes indicate unfavorable regions. (**c**) Overlay of molecules **2** (green ball stick), **62** (magenta ball stick), **9** (blue ball stick) aligned with AADRR pharmacophore model. Curved line represents second structure of Hsp90α

Validation of pharmacophore model

Twenty molecules in the test set were used to validate the predictive ability of this hypothesis. The PLS parameters are shown in Table 1. The observed and predicted activities obtained from the model are listed in Table S2. And visual representation of atom-based QSAR model is illustrated in Fig. 2b, where blue cubes represent regions of favorable interactions for activity, and red cubes are on the contrary.

Interpretation of the pharmacophore by superimposing with cocrystal complex

Pharmacophores located in the proximity, may correspond to the key residues of the receptor. As the initial conformations were derived from the crystal structures, we put the common hypothesis aligned conformations of active molecules **2**, **62** and **9** into the binding pocket of cocrystallized Hsp90α complex. We compared the pharmacophore model with the experimental intermolecular interactions. Figure 2c shows the overlay of these structures. A low RMSD value of 0.343 Å was determined between the conformation and the cocrystallized structure of molecule **2**. Particularly, the NH and CO groups in the 5-amides moiety superimposed the H-bond donor (N-H) and acceptor (C=O) features in the active molecules closely correspond to that of the residues (Gly97, Lys58).

Binding mode analysis by docking

The extra precision (XP) glide docking was used to predict binding modes and rank the docked poses. Firstly, we redocked the cocrystal ligand with a low RMSD of 0.493 Å. Then all 94 molecules were docked by the same method. The docking sores are listed in Table S2. It can be seen that most of the molecules bind to Hsp90 well, but several with low scoring, such as molecules **32**, **34**, **79** and **94**. This ascribes to the bulky and complex substituents of side chains, which are unfavorable to binding affinity.

Table 1 Summary of PLS analysis results for the AADRR pharmacophore model

Factors	SD	R-squared	F	P	Stability	RMSE	Q-squared	Pearson-R
1	0.6147	0.7301	192.1	7.05E-22	0.9859	0.5052	0.6745	0.8432
2	0.4721	0.8431	188.0	7.08E-29	0.9193	0.5090	0.6696	0.8501
3	0.3471	0.9164	252.1	4.23E-37	0.8607	0.3891	0.8069	0.9114
4	0.3036	0.9370	252.7	5.06E-40	0.8572	0.3703	0.8251	0.9203
5	0.2629	0.9534	274.3	3.46E-43	0.8366	0.3863	0.8097	0.9197

The binding modes of Hsp90α inhibitors were analyzed by molecules with different 4-position side chain based on the pyrazole and isoxazole scaffords, including the aryl, amino, carboxamide pyrazoles and aryl isoxazoles. In Fig. 3a, the docking results indicate that all molecules show similar binding poses in the ATP active site of human Hsp90α N-terminus. In Fig. 3b and c, it is observed that the identical pyrazole and isoxazole nitrogen atoms form a network of hydrogen bonds with the active site amino acids Thr184 and Gly97, together with water molecules within the binding pocket. And the 3-resorcinol moiety is positioned in the active site region, reported originally occupied by the adenine ring [49], which forms two H-bonds, *viz* one directly with Asp93 and one with Ser52 mediated by waters. The 5-amide carbonyl moiety interacts with Lys58 side chain and amide moiety contacts the backbone oxygen atom of Gly97, while the ethyl terminal take *van der Waals* contacts with Ile96. Hydrophobic interactions are also involved, including those residues which are located on the perimeter of the cavity. The chlorine substitutive position on resorcinol pointed directly toward the hydrophobic cavity formed by Leu48, Phe138, and Val150 (Fig. 3b). Replacement of the chlorine of the resorcinol ring by alkyl group results in an additional hydrophobic interaction with Leu107 in the flexible lipophilic pocket (Fig. 3c).

CoMFA and CoMSIA statistical results

The CoMFA and CoMSIA analyses were performed corresponding to the three strategies mentioned earlier. The statistical parameters of all the models are summarized in Table 2. The DBA strategy built the best CoMFA (q^2= 0.782, ONC=5 and r^2=0.923) and CoMSIA (q^2=0.829, ONC=6 and r^2=0.968) model. Moreover, it gave the bootstrapped r^2_{boot} of 0.935±0.018, 0.979±0.007 and SEE_{boot} of 0.304±0.160, 0.175±0.101 for CoMFA and

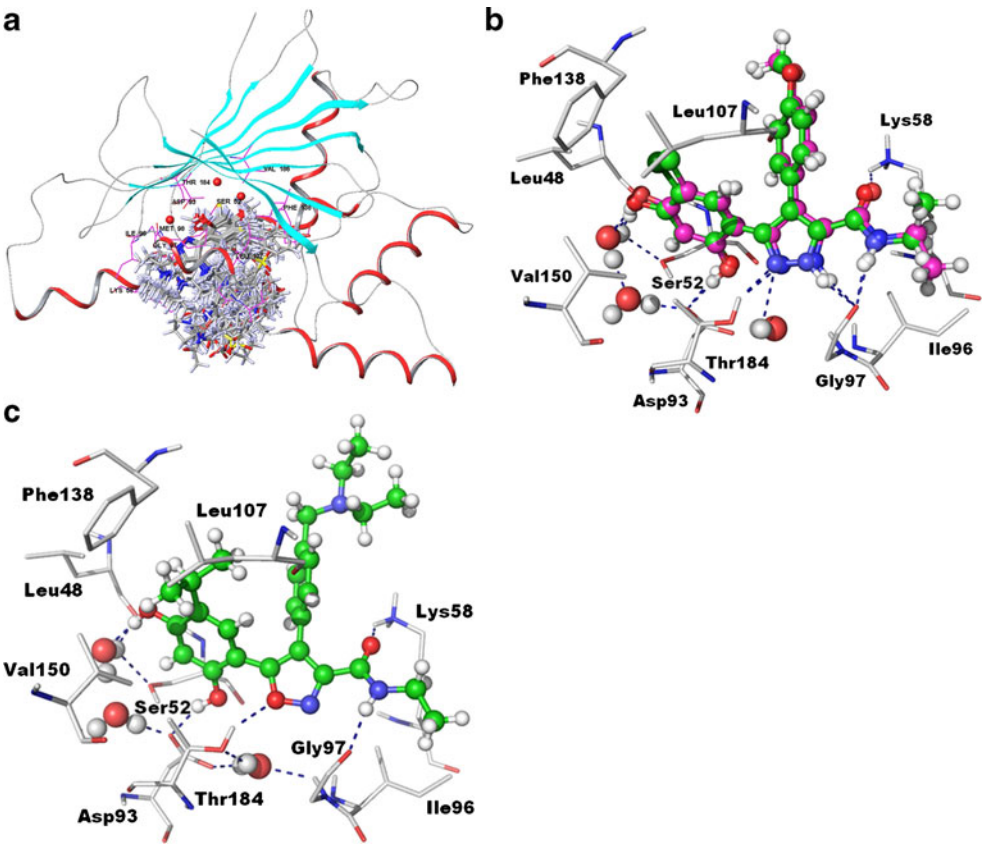

Fig. 3 Binding mode of inhibitors in Hsp90 active site: (**a**) Conformations of all docked molecules (**b**) Redocked molecule **2** (magenta) with the cocrystal ligand (green) (**c**) the most active molecule **62** (green). Red balls represent waters, and H-bond interactions are blue dots

Table 2 Summary of PLS analysis results for CoMFA and CoMSIA models

PLS	CoMFA			CoMSIA		
	CBA	PBA	DBA	CBA	PBA	DBA
q^2 [a]	0.767	0.77	0.775	0.769	0.784	0.829
ONC [b]	3	4	4	4	6	6
r^2_{tr} [c]	0.906	0.909	0.909	0.939	0.968	0.968
SEE_{tr} [d]	0.368	0.365	0.363	0.297	0.221	0.219
F [e]	223.899	169.321	173.067	267.794	328.834	335.966
r^2_{boot} [f]	0.931±0.017	0.941±0.017	0.935±0.018	0.959±0.012	0.975±0.008	0.979±0.007
SEE_{boot} [g]	0.312±0.153	0.292±0.149	0.304±0.160	0.241±0.121	0.190±0.103	0.175±0.101
r^2_{pred} [h]	0.856	0.709	0.837	0.856	0.809	0.871
SEE_{ts} [i]	0.413	0.500	0.423	0.409	0.681	0.406
field	contribution	[j]				
S	0.381	0.342	0.562	0.101	0.138	0.126
E	0.619	0.658	0.438	0.283	0.239	0.252
H	—	—	—	0.254	0.262	0.288
D	—	—	—	0.187	0.178	0.176
A	—	—	—	0.175	0.182	0.159

[a] Cross-validated correlation coefficient after leave-one-out procedure

[b] Optimal number of principal components

[c] Non-cross-validated correlation coefficient

[d] Standard error of estimate

[e] Ratio of r^2 explained to unexplained=$r^2/(1-r^2)$

[f] Average of correlation coefficient for 100 samplings using the bootstrapped procedure

[g] Average standard error of estimate for 100 samplings using the bootstrapped procedure

[h] Predicted correlation coefficient for the test set

[i] Standard error of estimate for the test set

[j] Abbreviations: S (steric); E (electrostatic); H (hydrophobic); D (H-bond donor); A (H-bond acceptor)

CoMSIA, respectively, which suggested that a good internal consistency existed within the training dataset.

For the three modeling approaches, the corresponding field contributions are listed in Table 2. It is observed that the electrostatic contributions are nearly twice the steric contributions in both CoMFA and CoMSIA results for the CBA and PBA. The steric and electrostatic contributions are similar in the CoMFA result and the electrostatic contributions are nearly twice the steric contributions in the CoMSIA for the DBA model. It is also observed that the hydrophobic contributions are the largest part in the CoMSIA models. The H-acceptor field has a similar contribution as does the H-donor field in the CoMSIA models. And the steric field seems to be weakened among the five terms. It is consistent with the significant hydrophobic effect and water bridge network in our previous docking study.

Validation of CoMFA and CoMSIA models

The predicted results for the test set are listed in Table 2. Both the DBA CoMFA and CoMSIA models give the highest r^2_{pred} with the lowest SEE_{ts}. The plot of the experimental versus the predicted pIC_{50} values for the training set and the test set is shown in Fig. 4, with ±1.2 and ±1.5 of triple values of standard error of estimation, respectively. The CoMSIA model gives the better relationship between the predictive r^2 with less residual values of the test set compared to the CoMFA model. The high predictive power of CoMFA and CoMSIA training models suggest that these models possess a high accommodating capacity and applicability in the development of new Hsp90α inhibitors. Since the DBA strategy shows the most significant statistic and prediction results, our discussion was focused on DBA models and their three-dimensional colored contour maps.

Interpretation of receptor-based CoMFA and CoMSIA contour maps

The steric and electrostatic contour maps of the docking-guided CoMFA and CoMSIA models are shown in Fig. 5a and b. The hydrophobic, H-bond donor and H-bond acceptor contour

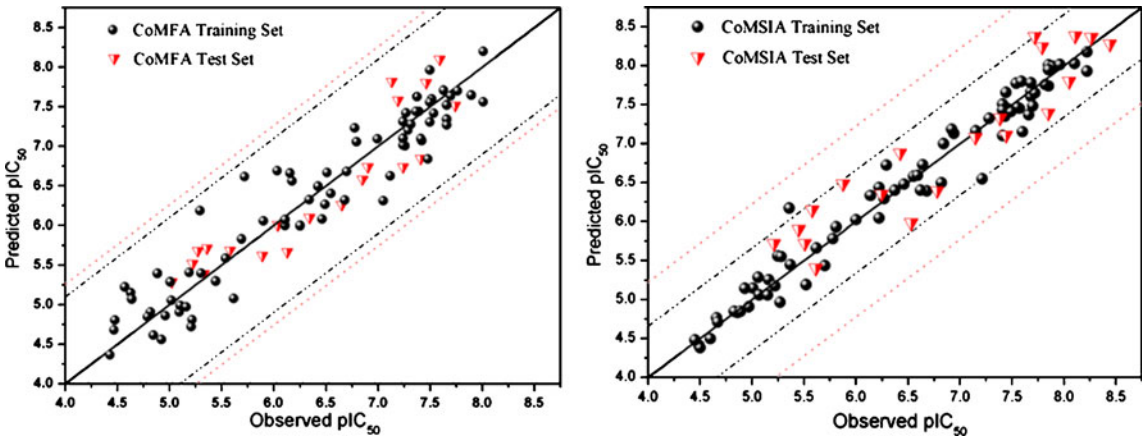

Fig. 4 Observed versus predicted pIC_{50} activity values for the training and test set of DBA models, where black dash dots represent triple values of *SEE* for training set, and red dots represent for test set

maps of CoMSIA are shown in Fig. 5c and d. Molecule **62** docked in the active site is used for further analysis.

In Fig. 5a and b, green contours represent bulky groups increase activity, while yellow contours represent bulky groups decrease activity for the steric field. Similarly blue contours indicate regions where electropositive groups increase activity, while red contours indicate regions where electronegative groups increase activity for the electrostatic field. For CoMFA steric field, two green and three yellow regions are recognized in the contour (Fig. 5a). Green contours appear near the 5-amide group and the *para* substituent of 4-position benzene ring, and they are also

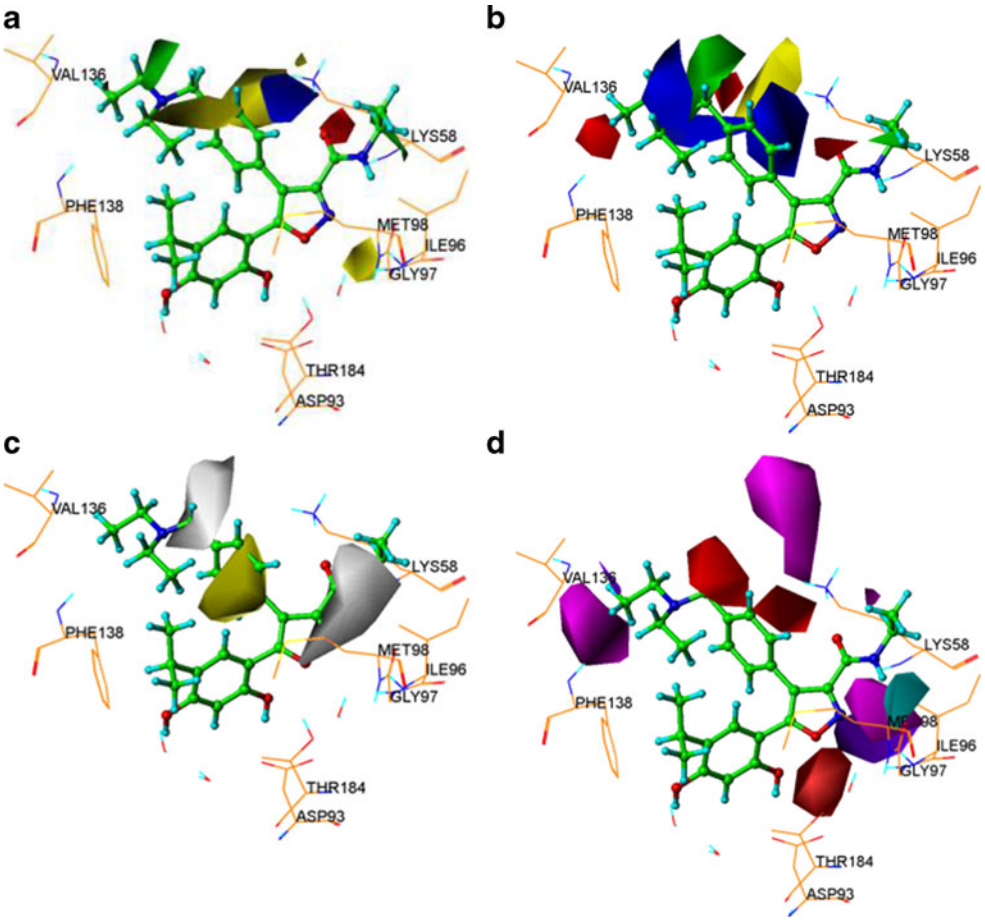

Fig. 5 CoMFA and CoMSIA STDEV*COEFF contour maps based on molecule 62 in the active site of Hsp90. CoMFA: (**a**) Steric and electrostatic fields. CoMSIA: (**b**) Steric and electrostatic fields. (**c**) Hydrophobic field. (**d**) H-bond acceptor and donor fields

found in the contour map of CoMSIA (Fig. 5b). This indicates that bulky groups in both positions can increase the activity. The observation correlates with the experimental determinations. For example, molecules **46**, **47** and **2** are more and more active after altering the R group from H to Ethyl. The *para*-substituted molecules (**5-11**, **63-71**, and **75-94**) show higher activity compared with those *meta* substituents (**12-20**, **72-74**). The residue Val136 is located to the outspread direction of the *para* position substituent, while Lys58 is close to the *meta* position of the binding pocket. Hence, there is not enough space for the bulky group of the *meta* position owing to the bad contact with Lys58, but the bulky group at *para* position is favorable for the interaction with Val136. In addition, the 4-amino analogues (molecules **21-39**) can increase activity by the bulkier *para* N-substituted group. Two yellow contours are observed around both sides of the *meta*-position of 4-position benzene ring. This suggests *meta*-position substitution is unfavorable for the activity. Another yellow region near the isoxazole ring is also steric-unfavorable. There is only a large yellow contour around the *meta*-position of 4-position benzene ring in the CoMSIA steric contour map.

For the CoMFA electrostatic contour map, the blue contour around the 4-position substituent demonstrates the positive-favorable property for inhibitory activity. This can be proved by the fact that molecule **27** is most potent among molecules **22-26**, **28**, **29**, while molecule **71** is of higher potency than molecules **15** and **17**. Molecules **4**, **50-61** with 4-carboxamides have lower activities than those with 4-phenyl rings. The red negative-favorable region is mainly on the carbonyl O of the 5-amides. These are also observed from the CoMSIA electrostatic contour map. Besides, a large blue contour placed between two red contours appears around the substituent -CH_2NEt_2 of 4-position phenyl group, which suggests electrostatic contributions have little effect to vary activity. In the CoMFA model, the contribution of electrostatic field is equal to that of steric field, but in the CoMSIA, the contribution of the electrostatic field is twice as much as the steric. As CoMFA does not have explicit hydrophobic and H-bond descriptors in the CoMSIA, which are assumed to be implicitly treated in the CoMFA steric and electrostatic fields, respectively, the electrostatic field component becomes higher in the CoMSIA.

In the CoMSIA hydrophobic contour (Fig. 5c), the white regions are in proximity to the polar pyrazole/isoxazole rings, 5-amides and 4-substitution moieties, which represent hydrophobic-disfavored for the activity. The yellow region overlaps the 4-phenyl group, which indicates this position is hydrophobic-favorable for the activity. Combining with the binding pocket, it can be seen that there is a crucial network of hydrogen bonding interactions involving the hydroxyl of 3-resorcinol and pyrazole/isoxazole ring with Asp93, Thr184 and a cluster of structurally conserved and highly ordered water molecules. The 4-aryl group is pointing toward the solvent in a quite open part of the binding site. The 5-amides group is close to the protein with a number of potential interaction sites and located in another solvent channel, which disfavors hydrophobicity. There is some but not large amounts of room near the region of the positive N of 4-substituted groups, which corresponds to the white region. The group at the position should be a proper one fitting into the binding site, not a large one.

As shown in H-bond donor and H-bond acceptor contour maps of CoMSIA (Fig. 5d), the cyan region of the H-bond donor favored, occurs over the 5-amides NH offered to interact with residue Gly97, whereas a purple H-bond donor disfavored contour occurs right closed to the two magenta H-bond acceptor favorable regions oriented above the C=O of 5-amides and between the C=O of 5-amides and the N of isoxazole ring. The red regions around 2-position hydroxyl of 3-resorcinol and the substituent -CH_2NEt_2 of 4-position phenyl group are unfavorable to the H-bond acceptor. The magenta contour with a small purple contour appears near the -CH_2NEt_2 group of 4-position phenyl, which is favorable to the H-bond acceptor. This probably reflects the polar substituents at the position providing potential H-bond acceptor for enhancing activity, such as active molecules **3**, **7-10** and **63-66**. In summary, the results of pharmacophore model, docking and 3D-QSAR are consistent and complimentary with each other. The detailed analyses as discussed above suggest important structural requirements for inhibitory activity. (Fig. 6).

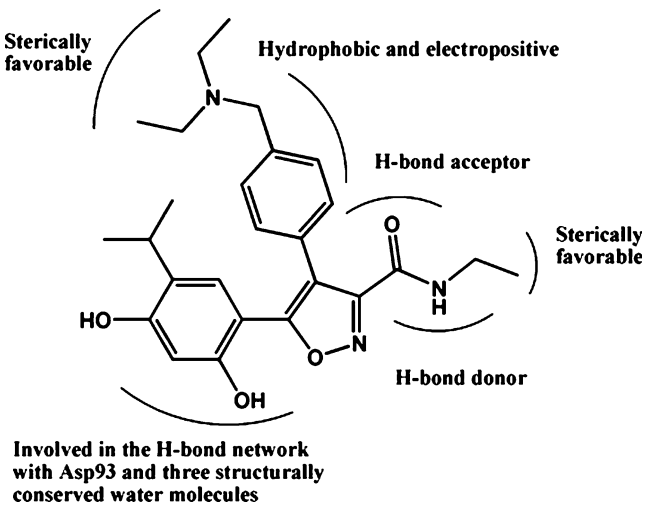

Fig. 6 Structural requirements for pyrazole/isoxazole based inhibitors for Hsp90α

Conclusions

In this study, we performed a combined molecular modeling study on a series of pyrazole-/isoxazole-based Hsp90α inhibitors by using pharmacophore model, molecular docking and 3D-QSAR. The obtained pharmacophore model provided the essential features for the inhibiting activity of these compounds. Molecular docking studies validated the identified pharmacophore features and also revealed that all the inhibitors showed similar binding mode with the key amino acid residues Lys58, Asp93, Gly97, Thr184 at the ATP binding site of human Hsp90α. Based on both ligand- and receptor-guided active conformational selection and alignment strategies derived from pharmacophore and docking analyses, 3D-QSAR models for Hsp90 inhibitors were developed. The results of receptor-based models indicated important requirements of H-bond donor/acceptor and hydrophobic groups. Substituent at 4-position is not merely just for filling the cavity in the active site, but also fulfills the electronic requirements. Bulkier electron-donating substituents at 4-aryl that can not give further interactions with important hydrophobic residues in the active site of Hsp90 are unfavorable for the ligand binding. Key H-bond donors and acceptors at 3-resorcinol and 5-amide which can form hydrogen bonds with the close residues increase the inhibitory activity. The obtained results from this combined molecular modeling study could provide useful information for the design of novel Hsp90α inhibitors as potential anticancer agents.

Acknowledgments This work was supported by the Program for New Century Excellent Talents in University (Grant No. NCET-07-0399) and the National Natural Science Foundation of China (Grant No. 20905033).

References

1. Whitesell L, Lindquist SL (2005) Hsp90 and the chaperoning of cancer. Nat Rev Cancer 5:761–772
2. Solit DB, Rosen N (2006) Hsp90: a novel target for cancer therapy. Curr Top Med Chem 6:1205–1214
3. Hadden MK, Lubbers DJ, Blagg BS (2006) Geldanamycin, radicicol, and chimeric inhibitors of the Hsp90 N-terminal ATP binding site. Curr Top Med Chem 6:1173–1182
4. Banerji U (2009) Heat shock protein 90 as a drug target: some like it hot. Clin Cancer Res 15:9–14
5. Chiosis G, Rodina A, Moulick K (2006) Emerging Hsp90 inhibitors: from discovery to clinic. Anticancer Agents Med Chem 6:1–8
6. Neckers L, Neckers K (2005) Heat-shock protein 90 inhibitors as novel cancer chemotherapeutics - an update. Expert Opin Emerg Drugs 10:137–149
7. Sharp S, Workman P (2006) Inhibitors of the HSP90 molecular chaperone: current status. Adv Cancer Res 95:323–348
8. Drysdale MJ, Brough PA (2008) Medicinal chemistry of Hsp90 inhibitors. Curr Top Med Chem 8:859–868
9. Kallblad P, Mancera RL, Todorov NP (2004) Assessment of multiple binding modes in ligand-protein docking. J Med Chem 47:3334–3337
10. Glen RC, Allen SC (2003) Ligand-protein docking: cancer research at the interface between biology and chemistry. Curr Med Chem 10:763–767
11. Barcellos GB, Pauli I, Caceres RA, Timmers LF, Dias R, de Azevedo WF Jr (2008) Molecular modeling as a tool for drug discovery. Curr Drug Targets 9:1084–1091
12. Chou KC, Wei DQ, Du QS, Sirois S, Zhong WZ (2006) Progress in computational approach to drug development against SARS. Curr Med Chem 13:3263–3270
13. Clark RD (2009) Prospective ligand- and target-based 3D QSAR: state of the art 2008. Curr Top Med Chem 9:791–810
14. Lauria A, Ippolito M, Almerico AM (2009) Principal component analysis on molecular descriptors as an alternative point of view in the search of new Hsp90 inhibitors. Comput Biol Chem 33:386–390
15. Morra G, Verkhivker G, Colombo G (2009) Modeling signal propagation mechanisms and ligand-based conformational dynamics of the Hsp90 molecular chaperone full-length dimer. PLoS Comput Biol 5:e1000323
16. Mitrasinovic PM (2010) Advances in the structure-based design of the influenza A neuraminidase inhibitors. Curr Drug Targets 11:315–326
17. Srinivas E, Murthy JN, Rao AR, Sastry GN (2006) Recent advances in molecular modeling and medicinal chemistry aspects of phospho-glycoprotein. Curr Drug Metab 7:205–217
18. Thomas MP, McInnes C (2006) Structure-based discovery and optimization of potential cancer therapeutics targeting the cell cycle. IDrugs 9:273–278
19. Williamson DS, Borgognoni J, Clay A, Daniels Z, Dokurno P, Drysdale MJ, Foloppe N, Francis GL, Graham CJ, Howes R, Macias AT, Murray JB, Parsons R, Shaw T, Surgenor AE, Terry L, Wang Y, Wood M, Massey AJ (2009) Novel adenosine-derived inhibitors of 70kDa heat shock protein, discovered through structure-based design. J Med Chem 52:1510–1513
20. Sgobba M, Rastelli G (2009) Structure-based and in silico design of Hsp90 inhibitors. Chem Med Chem 4:1399–1409
21. Pfisterer H, Wolber G, Efferth T, Rollinger M, Stuppner H (2010) Natural products in structure-assisted design of molecular cancer therapeutics. Curr Pharm Des 16:1718–1741
22. Spitzer GM, Heiss M, Mangold M, Markt P, Kirchmair J, Wolber G, Liedl KR (2010) One concept, three implementations of 3D pharmacophore-based virtual screening: distinct coverage of chemical search space. J Chem Inf Model 50:1241–1247
23. Brough PA, Barril X, Beswick M, Dymock BW, Drysdale MJ, Wright L, Grant K, Massey A, Surgenor A, Workman P (2005) 3-(5-Chloro-2, 4-dihydroxyphenyl)-pyrazole-4-carboxamides, as inhibitors of the Hsp90 molecular chaperone. Bioorg Med Chem Lett 15:5197–5201
24. Dymock BW, Barril X, Brough PA, Cansfield JE, Massey A, McDonald E, Hubbard RE, Surgenor A, Roughley SD, Webb P, Workman P, Wright L, Drysdale MJ (2005) Novel, potent small-molecule inhibitors of the molecular chaperone Hsp90 discovered through structure-based design. J Med Chem 48:4212–4215
25. Barril X, Beswick MC, Collier A, Drysdale MJ, Dymock BW, Fink A, Grant K, Howes R, Jordan AM, Massey A, Surgenor A, Wayne J, Workman P, Wright L (2006) 4-amino derivatives of the Hsp90 inhibitor CCT018159. Bioorg Med Chem Lett 16:2543–2548
26. Brough PA, Aherne W, Barril X, Borgognoni J, Boxall K, Cansfield JE, Cheung KM, Collins I, Davies NG, Drysdale MJ, Dymock B, Eccles SA, Finch H, Fink A, Hayes A, Howes R, Hubbard RE, James K, Jordan AM, Lockie A, Martins V, Massey A, Matthews TP, McDonald E, Northfield CJ, Pearl LH,

Prodromou C, Ray S, Raynaud FI, Roughley SD, Sharp SY, Surgenor A, Walmsley DL, Webb P, Wood M, Workman P, Wright L (2008) 4, 5-diarylisoxazole Hsp90 chaperone inhibitors: potential therapeutic agents for the treatment of cancer. J Med Chem 51:196–218
27. Sybyl, version 6.9 (1999) Tripos Associates, St. Louis, (MO)
28. Phase, version 3.0 (2008) Schrödinger, LLC, New York, NY
29. Ståhle L, Wold S (1987) Partial least squares analysis with cross-validation for the two-class problem: a Monte Carlo study. J Chemom 1:185–196
30. Glide, version 5.0 (2008) Schrödinger, LLC, New York, NY
31. Maestro, version 8.5 (2008) Schrödinger, LLC, New York, NY
32. Impact, version 5.0 (2005) Schrödinger, LLC, New York, NY
33. Friesner R, Murphy R, Repasky M, Frye L, Greenwood J, Halgren T, Sanschagrin P, Mainz D (2006) Extra precision glide: docking and scoring incorporating a model of hydrophobic enclosure for protein-ligand complexes. J Med Chem 49:6177–6196
34. Corbeil CR, Moitessier N (2009) Docking ligands into flexible and solvated macromolecules. 3. Impact of input ligand conformation, protein flexibility, and water molecules on the accuracy of docking programs. J Chem Inf Model 49:997–1009
35. Cao H, Cao R, Zhang H, Zheng X, Gao D (2008) Non-nucleoside inhibitors of NS5B polymerase binding to allosteric sites: 3D-QSAR and molecular docking studies. Curr Med Chem 15:1462–1477
36. Zhu LL, Hou TJ, Chen LR, Xu XJ (2001) 3D QSAR analyses of novel tyrosine kinase inhibitors based on pharmacophore alignment. J Chem Inf Comput Sci 41:1032–1040
37. Chen Y, Li H, Tang W, Zhu C, Jiang Y, Zou J, Yu Q, You Q (2009) 3D-QSAR studies of HDACs inhibitors using pharmacophore-based alignment. Eur J Med Chem 44:2868–2876
38. Aparna V, Jeevan J, Ravi M, Desiraju GR, Gopalakrishnan B (2006) 3D-QSAR studies on antitubercular thymidine monophosphate kinase inhibitors based on different alignment methods. Bioorg Med Chem Lett 16:1014–1020
39. Chung JY, Pasha FA, Cho SJ, Won M, Lee JJ, Lee K (2009) Pharmacophore-based 3D-QSAR of HIF-1 inhibitors. Arch Pharm Res 32:317–323
40. Patel PD, Patel MR, Kaushik-Basu N, Talele TT (2008) 3D QSAR and molecular docking studies of benzimidazole derivatives as hepatitis C virus NS5B polymerase inhibitors. J Chem Inf Model 48:42–55
41. Dessalew N, Patel DS, Bharatam PV (2007) 3D-QSAR and molecular docking studies on pyrazolopyrimidine derivatives as glycogen synthase kinase-3beta inhibitors. J Mol Graph Model 25:885–895
42. Vaidya M, Weigt M, Wiese M (2009) 3D-QSAR with the aid of pharmacophore search and docking-based alignments for farnesyltransferase inhibitors. Eur J Med Chem 44:4070–4082
43. Zhou Z, Madura JD (2004) CoMFA 3D-QSAR analysis of HIV-1 RT nonnucleoside inhibitors, TIBO derivatives based on docking conformation and alignment. J Chem Inf Comput Sci 44:2167–2178
44. Buolamwini JK, Assefa H (2002) CoMFA and CoMSIA 3D-QSAR and docking studies on conformationally-restrained cinnamoyl HIV-1 integrase inhibitors: exploration of a binding mode at the active site. J Med Chem 45:841–852
45. Cramer RD III, Patterson DE, Bunce JD (1988) Comparative molecular field analysis (CoMFA). I. Effect of shape on binding of steroids to carrier proteins. J Am Chem Soc 110:5959–5967
46. Klebe G, Abraham U, Mietzner T (1994) Molecular similarity indices in a comparative analysis (CoMSIA) of drug molecules to correlate and predict their biological activity. J Med Chem 37:4130–4146
47. Wold S (1978) Cross validatory estimation of the number of components in factor and principal components models. Technometrics 20:397–405
48. Cramer RD III, Bunce JD, Patterson DE, Frank IE (1988) Crossvalidation, bootstrapping, and partial least squares compared with multiple regression in conventional QSAR studies. Quant Struct Act Relat 7:18–25
49. Messaoudi S, Peyrat JF, Brion JD, Alami M (2008) Recent advances in Hsp90 inhibitors as antitumor agents. Anticancer Agents Med Chem 8:761–782